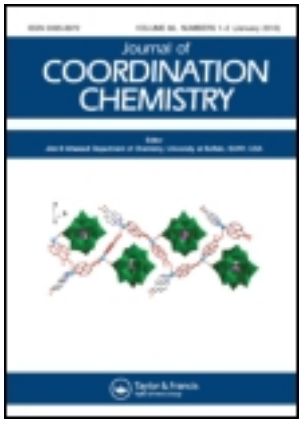

Journal of Coordination Chemistry
Publication details, including instructions for authors and subscription information:
http://www.tandfonline.com/loi/gcoo20

A new 1H-pyridin-(2E)-ylidene ruthenium complex as sensitizer for a dye-sensitized solar cell

Cigdem Sahin [a], Canan Varlikli [b], Ceylan Zafer [b], Qi Shi [c] & Richard E. Douthwaite [c]

[a] Art & Science Faculty, Department of Chemistry, Pamukkale University, Denizli, Turkey

[b] Solar Energy Institute, Ege University, Izmir, Turkey

[c] Department of Chemistry, University of York, York, UK

Accepted author version posted online: 06 Mar 2013.Published online: 09 Apr 2013.

Journal of Coordination Chemistry, 2013
Vol. 66, No. 8, 1384–1395, http://dx.doi.org/10.1080/00958972.2013.782486

A new 1*H*-pyridin-(2E)-ylidene ruthenium complex as sensitizer for a dye-sensitized solar cell

CIGDEM SAHIN*†, CANAN VARLIKLI‡, CEYLAN ZAFER‡, QI SHI§ and RICHARD E. DOUTHWAITE§

†Art & Science Faculty, Department of Chemistry, Pamukkale University, Denizli, Turkey; ‡Solar Energy Institute, Ege University, Izmir, Turkey; §Department of Chemistry, University of York, York, UK

(*Received 2 August 2012; in final form 17 January 2013*)

The new heteroleptic ruthenium(II) complex containing a 1*H*-pyridin-(2E)-ylidene (PYE) ligand was synthesized and characterized using UV/Vis, FTIR, and NMR spectroscopies, mass spectrometry, elemental analysis, and cyclic voltammetry. The photovoltaic performance of the ruthenium complex as a charge transfer photosensitizer in *nc*-titanium dioxide based dye-sensitized solar cell was studied and compared with *cis*-bis(isothiocyanato)(2,2′-bipyridyl-4,4′-dicarboxylato)(2,2′-bipyridyl-4,4′-di-nonyl)ruthenium(II) (Z907) under standard AM 1.5 sunlight. The complex CS90 gave a photocurrent density of 1.80 mA cm^{-2}, 400 mV open-circuit potential, and 0.58 fill factor yielding an efficiency of 0.42% where the reference Z907 yielded an efficiency of 4.12%. The decrease in conversion efficiency observed for CS90 is attributed to a steric interaction between PYE and the TiO_2 surface that prevents optimum binding and also restricts ligand dynamics that are associated with oxidation state changes.

Keywords: 1*H*-Pyridin-(2E)-ylidene; Ruthenium(II) complexes; Dye-sensitized solar cells

1. Introduction

Nanocrystalline titanium dioxide (*nc*-TiO_2)-based dye-sensitized solar cells (*nc*-DSSCs) convert sunlight to electricity and have interest for energy applications [1, 2]. The most conspicuous advantages of these devices are their low manufacturing cost compared to traditional solid state, crystalline silicon solar cells, and their efficiency under diffuse illumination [3–6]. In *nc*-DSSCs, the dye is the key component for light collection to support high-power conversion efficiencies, and therefore, the development of new dyes to improve performance has received considerable attention [7, 8]. Of the dye materials investigated to date, polypyridyl ruthenium(II) complexes containing 4,4′-dicarboxy-2,2′-bipyridine as a photosensitizer attached to nanocrystalline TiO_2 are the most widely studied ones in solar energy conversion due to their stability, photophysical, photochemical, and electrochemical properties [9–11].

Amphiphilic heteroleptic sensitizers containing donor ligands have several advantages in *nc*-DSSC, such as: (i) increasing the dye loading onto the TiO_2 surface by reducing

*Corresponding author. Email: csahin@pau.edu.tr

repulsive electrostatic interactions between dyes [12], (ii) increasing the pK_a of the dicarboxylates, which results in stronger binding [13], (iii) shifting the oxidation potential of the heteroleptic complexes cathodically, which increases the oxidation reversibility of the ruthenium III/II couple leading to enhanced stability [13]. Given these considerations we investigate the synthesis of heteroleptic ruthenium(II) complex containing the 1*H*-pyridin-(2E)-ylidene (PYE) (**A**) (Figure 1), which can be prepared from a wide range of primary amines [14]. These ligands are strong donors via conjugation between the *N*-heterocycle and imine moieties, giving a contribution of the azolium-amido resonance structure (**B**) to the metal-ligand bonding (Figure 1) [14].

In this paper, we report the synthesis and characterization of a new quinoline based PYE ligand and a heteroleptic ruthenium(II) complex derivative, CS90, and its subsequent application to *nc*-DSSCs. The motivation was to explore if the strongly donating PYE could be incorporated into the sensitizer and cathodically shift the ruthenium II/III redox couple. The photovoltaic performance of the ruthenium complex (CS90) as a charge transfer photosensitizer in a *nc*-DSSC was also studied and compared with the established sensitizer *cis*-bis(isothiocyanato)(2,2′-bipyridyl-4,4′-dicarboxylato)(2,2′-bipyridyl-4,4′-di-nonyl) ruthenium(II) (Z907).

2. Experimental

2.1. *Materials*

Ammonium thiocyanate, tetrabutyl ammonium hexafluorophosphate ($TBAPF_6$), and triethylamine were purchased from Fluka. Dichloro(*p*-cymene) ruthenium(II) dimer, LH-20 Sephadex gel, 4,4′-dimethyl-2,2′-bipyridine, 8-aminoquinoline, 2-chloro-1-methyl-pyridinium iodide, sodium hydroxide, 1-butyl-3-methylimidazolium iodide, lithium iodide, iodine, trifluoroacetic acid (TFA) and tert-butyl pyridine were obtained from Aldrich. Titanium tetra iso-propoxide [$Ti(OPri)_4$] was obtained from Acros. *cis*-Bis(isothiocyanato)(2,2′-bipyridyl-4,4′-dicarboxylato)(2,2′-bipyridyl-4,4′-di-nonyl)ruthenium(II) (Z907) was provided by Solaronix. All reactions and manipulations were carried out under argon using standard Schlenk techniques. Solvents were dried and distilled under a nitrogen atmosphere prior to use. All other chemicals were used as received.

2.2. *Measurements*

UV–vis spectra were recorded in a 1-cm path length quartz cell using an Analytic Jena S 600 UV diode array spectrophotometer. The spectra were measured in *N*,*N*-dimethylformamide (DMF) at a concentration of 0.04 mM. Infrared spectra were recorded on a

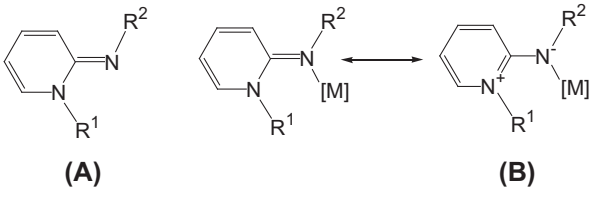

Figure 1. Resonance structures of 1*H*-pyridin-(2E)-ylidene on coordination to a metal fragment [14].

PerkinElmer, Spectrum BX-FTIR spectrophotometer as a KBr disk. The attenuated total reflection-Fourier transform infrared (ATR-FTIR) spectrum was measured using a diamond anvil ATR accessory with 64 scans at a resolution of 2 cm^{-1}. NMR spectra were recorded at probe temperature on a JEOL 400 instrument. The reported chemical shifts are referenced to tetramethylsilane. Elemental analyses were performed using a Carlo Erba 1106 elemental analyzer. Mass spectra were recorded on a Bruker Esquire 6000 ESI spectrometer using methanol as the mobile phase. Electrochemical data were obtained using a CH Instrument 660 B Model Electrochemical Workstation. Cyclic voltammograms were measured in a cell containing a glassy carbon working electrode, silver wire reference electrode, platinum wire counter electrode, and supporting electrolyte consisting of 0.1 M $TBAPF_6$ in DMF with a scan rate of 100 mVs^{-1}. The thickness and morphology of the *nc*-TiO_2 layers were measured using an Ambios XP-1 high resolution profilometer and Ambios QScope 250 model atomic force microscope (AFM), respectively. Photovoltaic data were obtained using a Keithley 2400 Source-Meter and Labview data acquisition system under dark and 100 mW cm^{-2} simulated white light irradiation using a KHS solar simulator equipped with a 750 W metal halide light source and AM1.5 global spectral distribution filter.

2.3. *Synthesis and characterization*

2.3.1. Synthesis of 4,4-dicarboxy-2,2-bipyridine (1). Starting from 4,4′-methyl-2,2-bipyridine, **1** was synthesized according to a literature procedure [15]. The product was purified and characterized as 4,4′-dicarboxy-2,2-bipyridine (**1**). 96% yield. FTIR (KBr, cm^{-1}): 1290, 1563, 1604, 1719, 3449. ^{1}H NMR (D_2O + NaOH, 400 MHz) δ ppm: 7.73 (d, J = 5.2, 2H, CC*H*CH); 8.24 (s, 2H, CC*H*C); 8.64 (d, J = 5.2, 2H, NC*H*CH). ^{13}C NMR (D_2O + NaOH, 100 MHz) δ ppm: 121.5; 123.5; 146.6; 149.9; 155.9; 173.2.

2.3.2. Synthesis of [1-methyl-1H-pyridin-(2E)-ylidene]-8-quinolinamine (2). 8-Aminoquinoline (2.0 g, 13.9 mmol) was added to an ampoule charged with 2-chloro-1-methylpyridinium iodide (3.54 g, 13.9 mmol), triethylamine (3.90 mL, 27.8 mmol) in acetonitrile (25 mL) and the mixture was stirred for 20 h at 80 °C. The volatiles were removed under reduced pressure and the solid was extracted with dichloromethane (80 mL),and filtered, and the filtrate was added into aqueous sodium hydroxide (50 mL, 5 M). The organic phase was separated and the aqueous phase was washed with dichloromethane (3 × 50 mL). Dichloromethane extracts were collected and the volatiles were removed under reduced pressure to give **2** as a dark brown solid. Yield = 3.26 g, 92%. ^{1}H NMR ($CDCl_3$, 400 MHz): 3.78 (s, 3H, NCH_3), 5.94 (m, 1H, py-H4), 6.20 (d, $^3J_{H-H}$ = 9 Hz, 1H, py-H2), 6.87 (m, 1H, py-H3), 7.26–7.32 (m, 3H, py-H5 + 2$CH_{quinolinyl}$), 7.41 (m, 2H, $CH_{quinolinyl}$), 8.04 (m, 1H, $CH_{quinolinyl}$), 8.73 (m, 1H, $CH_{quinolinyl}$); $^{13}C\{^1H\}$ NMR (100 MHz, $CDCl_3$): 41.1 (NCH_3), 105.5 (py-C4), 115.1 (py-C2), 121.0, 121.6, 122.1, 127.2, 129.6136.3 (py-C3), 136.4, 139.2 (py-C5), 142.7, 145.6, 149.0, 153.4 (py-C1); MS (ESI) *m/z* (%): 236.0 ($[M+H]^+$, 100%); Anal. Calcd for $C_{15}H_{13}N_3$ (%): C, 76.59; H, 5.56; N, 17.71. Found: C, 76.57; H, 5.57; N, 17.86.

2.3.3. Synthesis of CS90. CS90 was prepared with a modified literature procedure used for the stepwise preparation of ruthenium bipyridine derivatives [13]. A mixture of $[RuCl_2(p\text{-cymene})]_2$ (0.20 g, 0.32 mmol) and **2** (0.15 g, 0.64 mmol) in DMF (40 mL) was

heated at 60 °C under argon for 4 h. Subsequently, **1** (0.16 g, 0.64 mmol) was added and the mixture refluxed for a further 4 h, followed by an excess of NH_4SCN (1.52 g, 19.92 mmol) and the reflux continued for a final 4 h. On cooling the volatiles were removed under reduced pressure and the residue was washed with water and collected by filtration. The crude complex was purified on a Sephadex LH-20 column using methanol as an eluent and on removal of the volatiles, CS90 was isolated as a brown powder. Yield = 154 mg, 50%. FTIR (KBr, cm^{-1}): 3421, 2110, 1954, 1707, 1627, 1554, 1491, 1462, 1442, 1375, 1232, 1161, 772. ^{1}H NMR (CD_3OD, 400 MHz) δ ppm: 9.59 (d, $^3J_{H-H}$ = 6.4 Hz, 1H), 9.05 (s, 1H), 8.98 (d, $^3J_{H-H}$=4.8 Hz, 1H), 8.89 (s, 1H), 8.84 (d, $^3J_{H-H}$ = 4.8 Hz, 1H), 8.48 (d, $^3J_{H-H}$ = 7.2 Hz, 1H), 8.35 (d, $^3J_{H-H}$ = 7.2 Hz, 1H), 8.29 (d, $^3J_{H-H}$ = 8.0 Hz, 1H), 8.19 (d, $^3J_{H-H}$ = 7.2 Hz, 1H), 7.75 (m, 1H), 7.54 (m, 2H), 7.40 (m, 1H), 7.21 (m, 2H), 6.89 (d, $^3J_{H-H}$ = 5.5 Hz, 1H), 4.25 (s, 3H). ESI-MS (*m/z*) 697.0 $[M+H]^+$. Anal. Calcd for $C_{29}H_{21}N_7O_4RuS_2$ (%): C, 49.99; H, 3.04; N, 14.07. Found: C, 49.93; H, 3.09; N, 14.01.

2.3.4. Construction of the nc-DSSC assembly. The TiO_2 electrodes and TiO_2 nanoparticle precursor were prepared using a literature procedure [5]. The surface morphology of the TiO_2 layer was investigated by AFM. AFM image of *nc*-TiO_2 layer (Figure 2) exhibits a homogeneous surface structure with 30 ± 5 nm diameter. TiO_2 electrodes were sensitized with dye by dipping in a 3 mM solution of dye in DMF for 6 h. The surface coverages of CS90 and Z907 dyes on TiO_2 were monitored as a function of the different concentrations (0.1, 1, 2, 3, 4, and 5 mM) of dye solutions. The equilibrium binding of CS90 and Z907 on TiO_2 was reached at 3 mM. The dye-coated electrodes were rinsed with acetonitrile and dried with a nitrogen gas flow at room temperature.

The DSSCs were prepared by placing the electrodes on top of each other in a sandwich geometry separated by thermoplastic Surlyn® 1702 (DuPont) polymer frame as sealant

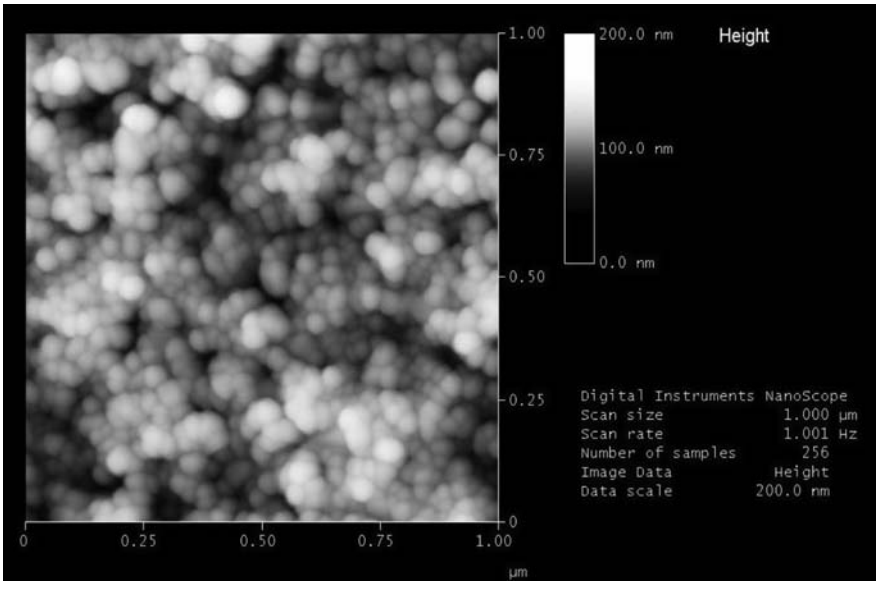

Figure 2. Atomic force microscopy (AFM) image of *nc*-TiO_2 film coated on FTO (SnO2: F) glass.

with thickness of 50 μm. The cell was sealed by heating the electrodes at 110 °C and pressing lightly on a hotplate and subsequently filled with iodide/triiodide redox couple and electrolyte by vacuum via a pre-drilled hole. The redox couple and electrolyte comprise 1-butyl-3-methyimidazolium iodide (0.6 M), lithium iodide (0.1 M), iodine (0.05 M), and tert-butyl pyridine (0.5 M) dissolved in 3-methoxy propyonitrile. The active area of the prepared solar cells was fixed at 1.0 cm^2 using a (square) mask.

In the presented work, all device parameters including TiO_2 nanoporous electrodes, Pt counter electrode, and electrolyte except dye were kept exactly the same with the reference in order to eliminate differences on charge transport, dye regeneration rates, and active surface area.

3. Results and discussion

3.1. *Synthesis, structural characterization, and binding to TiO_2*

The synthesis of the CS90 that is the focus of this study is shown in scheme 1. The proposed formulation and purity of CS90 were confirmed by a combination of spectroscopic, mass spectrometry, and bulk elemental analysis. ESI-mass spectrometry gave the parent molecular ion $[M+H]^+$ at *m/z* 697 and ^1H NMR spectroscopy showed signals attributable to the *N*-heterocyclic moieties **1** and **2** including a singlet at δ 4.25 ppm attributable to the methyl substituent of **2**. The possible geometric isomers were identified using IR spectroscopy. The spectrum (Supplementary material) exhibits two bands centered at 2111 and 1954 cm^{-1}, characteristic for *cis* thiocyanates [5, 16]. *N*-coordination of the thiocyanate is confirmed by the presence of ν(C=S) at 772 cm^{-1} [13, 16].

There remain two possible isomers that are distinguished by coordination of the imine functionality of **2** *trans* to a thiocyanate or bipyridine. Related classes of complex that contain mixtures of bipyridine, phenanthroline, and phenazine typically show thiocyanate IR stretches between ca. 2100–2130 and 1980 and 2090 cm^{-1}, respectively [16, 17], whereas for **2** a significantly lower stretch at 1954 cm^{-1} is observed. It has been shown [18] that PYE present in **2** is a much stronger donor than pyridine and related N-donor ligands and a poorer π-acceptor. Therefore, the most thermodynamically stable isomer will likely contain the imine functionality of **2** *trans* to a thiocyanate as shown in scheme 1 [19].

The peaks at 1708 and 3421 cm^{-1} are assigned to ν(C=O) and ν(O–H) from the carboxylic acid, respectively. The peak at 1627 cm^{-1} is due to the exocyclic ν(C=N) of **2** [20, 21]

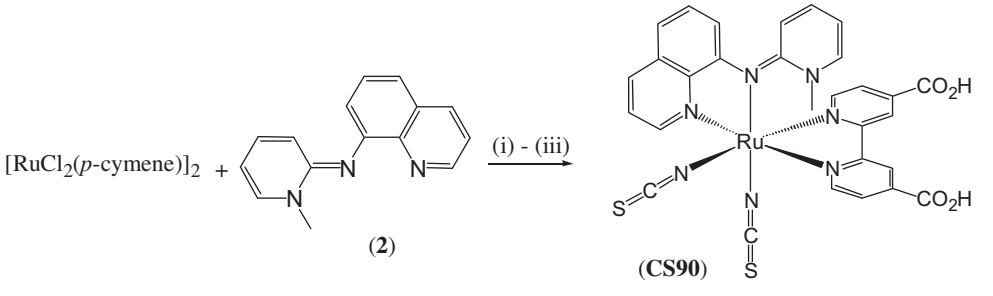

Scheme 1. The synthesis of CS90: (i) DMF, 60 °C, 4 h; (ii) L_1, reflux, 4 h; (iii) NH_4NCS, reflux, 4 h.

and the remaining peaks are attributable to ν(C–O) and ring stretch of the ligands [5]. ATR-FTIR spectrum of the CS90 dye adsorbed onto TiO_2 film (Supplementary material) shows a broadening of all signals that are attributable to adsorption on the TiO_2 surface via the carboxyl functionalities. There has been significant debate with respect to surface binding modes of dyes incorporating two bipyridine dicarboxylic acids, where most conceivable variations have been suggested, indicating that a single mode is probably not common to all systems [22]. With respect to dyes containing a single dicarboxylic acid ligand there is evidence to suggest that surface attachment occurs via a bidentate coordination (–CO_2)–Ti and monodentate (–CO(OH))–Ti hydrogen bond, respectively [22]. For CS90, strong bands are observed at 1772 and 1250 cm^{-1} which is strongly suggestive of an ester-like bonding interaction. This is attributed to the C=O stretch of a carboxylic acid on TiO_2 film at a higher wavenumber (1772 cm^{-1}). The C=O stretch of the monodentate ester-like bond is at a higher wavenumber than the C=O stretch of dye molecules, whereas the band at 1605 cm^{-1} is assigned to chelation or bridging modes to a semiconductor surface [23, 24]. The strong bands at 2700 and 1704 cm^{-1} indicate a hydrogen-bonding carboxylic acid. It is therefore suggested that binding occurs predominantly between both carboxylic acid functionalities and the surface via monodentate coordination (–CO_2)–Ti and hydrogen-bonding interaction, respectively. However, the peak broadness indicates some contribution via bidentate (–CO_2)–Ti, which is plausible given that a rough TiO_2 surface will present optimum bond distance and angles to maximize binding strength via monodentate and bidentate –CO_2^- bonding. In contrast in the IR spectrum of Z907 dye adsorbed onto TiO_2, carboxylate bands at 1607 and 1379 cm^{-1} indicate that both carboxylic acid groups are involved in adsorption to the TiO_2 surface [13, 25] and are interpreted as exhibiting bridging unidentate (–CO_2)–Ti [8, 26]. It is clear from the IR spectrum of CS90 adsorbed onto TiO_2 that bridging unidentate coordination does not occur for CS90 on TiO_2. This result indicates that steric effect of PYE of CS90 may prevent optimum binding of the carboxylate on TiO_2. It was reported [14] that the lack of rotation about exocyclic C–N bond and the disposition of N–CH_3 in the vicinity of metal causes steric effect in PYE. The steric effect of ligand causes change in the geometry, electrochemical properties, and energetics of the compounds [27]. This may affect the binding of carboxylate on TiO_2 and steric effect decreases formation of TiO_2–COOH bonding [28].

The adsorption of dye molecules on TiO_2 was measured according to a literature procedure [3]. The equilibrium surface coverages of CS90 and Z907 on TiO_2 film (Figure 3) are 1.0×10^{-7} and 1.7×10^{-7} mol cm^{-2}, respectively. The difference of surface coverage can be attributed to the molecular structure of CS90 dye that sterically inhibits its sensitization efficiency in comparison with Z907 dye [29].

3.2. *UV–vis absorption studies*

UV–vis absorption spectra of CS90 in DMF and adsorbed on a *nc*-TiO_2 film are shown in Figure 4, and maximum absorption wavelengths and the corresponding decadic molar extinction coefficients are summarized in Table 1 in comparison with the reference dye Z907. The absorption spectrum of CS90 in DMF showed bands at 370, 463 and 534 nm that are assigned to metal-to-ligand charge transfer (MLCT) bands based on reported spectra of related complexes [13, 26, 30]. Bands in the UV region, at 269 and 309 nm, correspond to the π–π^* transitions of **2** and **1**, respectively. In comparison with Z907, the lowest-energy MLCT band of CS90 is red shifted by 10 nm while the molar extinction coefficient decreases

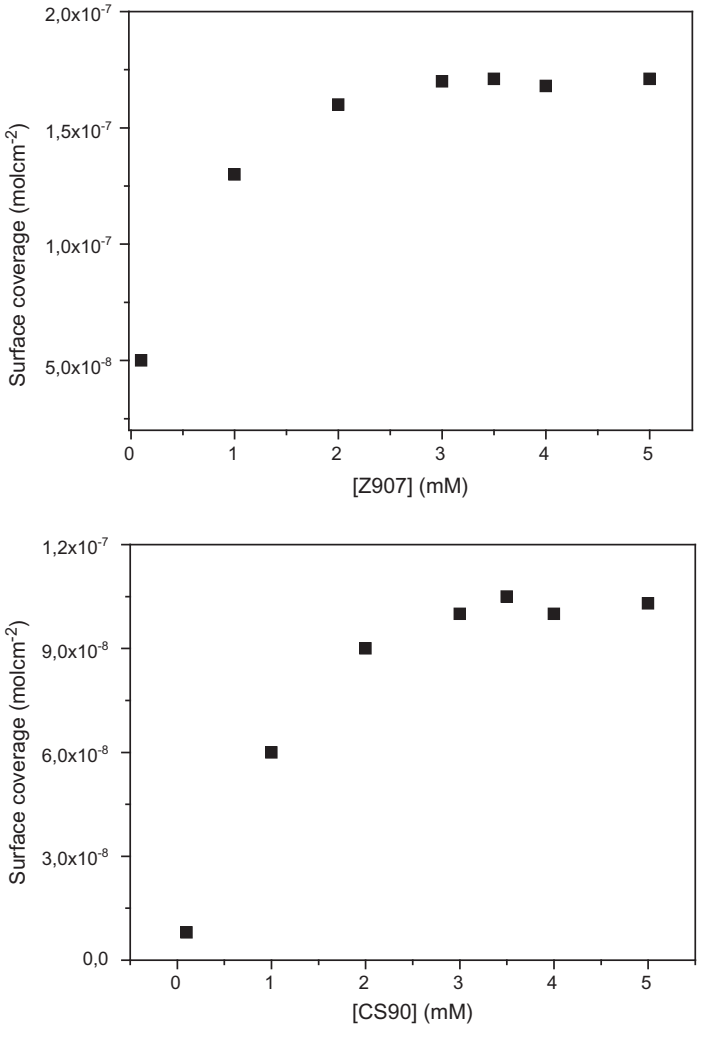

Figure 3. The surface coverages of CS90 and Z907 dyes on TiO_2 as a function of the different concentrations (0.1, 1, 2, 3, 4, and 5 mM) of dye solutions.

by 1.5-fold. The red shift is attributed to poorer π-acceptor character of **2** which would result in a slight increase in energy of the metal-based HOMO relative to the bipyridine-based LUMO [5, 16].

A red shift is also observed in the absorption spectra of CS90 adsorbed on a 4-m thick *nc*-TiO_2 electrode film (Figure 4(b)) with the low-energy MLCT maximum at 544 nm. This is due to electron withdrawing effect of the Ti^{4+} ions on binding of the dye to the TiO_2 surface, relative to the protonated carboxylate precursor [5, 26].

3.3. *Electrochemical data*

Electrochemical studies were performed by cyclic voltammetry in DMF using a glassy carbon and silver wire as working and reference electrodes, respectively. Votammograms

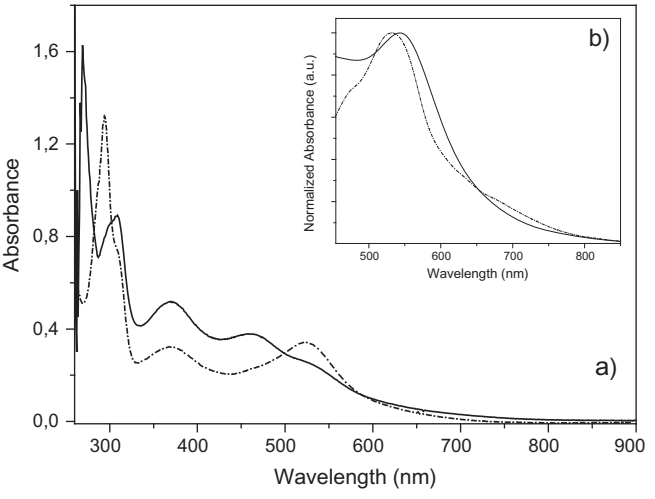

Figure 4. (a) UV–vis absorption spectra of 4×10^{-5} M solution of CS90 (solid line) and Z907 (dotted line) complexes in DMF, (b) UV–vis absorption spectra of CS90 (solid line) and Z907 (dotted line) dyes adsorbed on 4 μm thick *nc*-TiO_2 film.

Table 1. Absorption and electrochemical data of CS90 and Z907 in DMF.

Complex	λ_{max} (nm) ($\varepsilon/10^4\,M^{-1}\,cm^{-1}$) π–π^*	d π–π^*	E_{red1} (V)	E_{red2} (V)	E_{red3} (V)	E_{ox1} (V)	E_{ox2} (V)
CS90	296 (4.10) 309 (2.25)	370 (1.33) 463 (0.95) 534 (0.63)	−1.48	−1.71	−2.01	0.94	1.15
Z907	267 (1.58) 300 (3.48)	374 (0.90) 524 (0.93)	−1.18	−1.41	−1.72	0.98	

are shown in Supplementary material and the data in Table 1. The differential cyclic voltammogram of CS90 (Supplementary material) shows two oxidation and three reduction peaks at 0.94, 1.15 and −1.48, −1.71, −2.01 V *versus* Ag/Ag^+, respectively. The peak at 0.65 V *versus* Ag/Ag^+ is due to ferrocenium/ferrocene couple, which was used as an internal reference standard. For Z907 the electrochemical data are consistent with that reported in the literature showing an oxidation peak at (0.98 V) due to ruthenium II/III couple and reduction peaks that are bipyridine based [13]. For CS90 the electrochemistry does not show the reversibility of Z907 but exhibits stable electrochemistry after the first cycle. In contrast to Z907, a much lower reduction peak at −2.01 V is observed which is consistent with reduction in a quinoline that is typically observed at ca. −2.0 V [26, 31]. With respect to oxidation chemistry, two oxidation couples at 0.94 and 1.15 V are observed, in contrast to the single oxidation observed for Z907 over the same range. The relationship between ruthenium oxidation potentials and ligand donor strength has been discussed previously [32]. In comparison with a bipyridyl ligand, the strongly donating PYE would increase the largely ruthenium-based HOMO energy level resulting in a cathodic shift for metal-based oxidations. Indeed, a cathodic shift of 40 mV is observed for CS90 in comparison with Z907 for the oxidation at 0.94 V which is attributed to a ruthenium II/III couple, and the oxidation at 1.15 V to ruthenium III/IV. Collectively, compared to Z907, the oxidation and ligand based reduction potentials of CS90 are shifted cathodically, which we attribute to

the strongly donating PYE of **2** and its poorer π-acceptor character, in comparison with a pyridyl of the bipyridine of Z907 [13, 14]. This indicates that both the HOMO and LUMO levels of CS90 are slightly higher in energy than for Z907.

The cyclic voltammogram of CS90 dye anchored onto a 4 m thick *nc*-TiO_2 film is shown in Supplementary Material. When the dye is adsorbed onto a *nc*-TiO_2 film, the redox couples broaden with a greater voltage difference between them. Z907 dye anchored on the surface of TiO_2 results in a 100 mV anodic shift of the oxidation potential at 1.08 V attributed to electron withdrawing of the TiO_2 surface compared to solution phase. In contrast, the first oxidation for CS90 is at 0.86 V with a 80 mV cathodic shift, whereas the second oxidation at 1.23 V is shifted anodically by 80 mV compared to the solution phase. This observation suggests that binding to the surface and geometrical modifications of the complex initially cause an increase in the HOMO energy level that on oxidation leads to significant lowering [27]. Molecular models of CS90 indicate that the *N*-methyl substituent of PYE is in close proximity to a pyridyl. The resulting strain and distortion of the Ru–N bond is seen in other complexes incorporating PYE which have been structurally characterized using X-ray diffraction [18]. Binding of the carboxylate functionalized bipyridine could potentially relieve some of this localized strain to increase the strength of the Ru–N interaction raising the HOMO.

3.4. *Photovoltaic performance*

Current density–voltage (*J–V*) curves of *nc*-DSSC sensitized with CS90 and Z907 are given in Figure 5, and the photovoltaic performance data are summarized in Table 2. As seen from Table 2, between the photovoltaic conversion efficiencies of CS90 and Z907-based *nc*-DSSCs, there is a surprisingly large difference. Under standard conditions with 100 mWcm^{-2} simulated white light illumination, CS90 yielded 0.42% conversion efficiency while that of Z907 was 4.12%. Although some differences were observed between the electrochemical and spectroscopic properties of the metal complexes, it is evident that for TiO_2 bound materials, electron injection is being compromised. The IR and electrochemical evidence of TiO_2 bound CS90 indicates that the PYE motif may exert sufficient steric pressure to prevent optimum binding of the carboxylate and steric pressure causes distortion within the complexes reducing the electron transfer. Also, cathodic shift in HOMO energy level of CS90 from 0.94 to 0.86 V (*versus* Ag/Ag^+) upon bonding to TiO_2 surface may slow the dye regeneration rate from the iodine-based redox couple which is 0.35 V (*versus* NHE), even though dye regeneration is still energetically favorable. On the other side, reduction potential of CS90 is relatively higher than the reduction potential of the reference Z907 dye, −1.48 and −1.18 V, respectively. 0.3 V difference between LUMO energy levels can affect electron injection rate from dye LUMO to TiO_2 CB. According to Moser and Gratzel, electron transfer rate decreases by several orders of magnitude with increasing driving force, which means electron transfer takes place in the inverted Marcus region [33, 34].

The effect of electrolyte pH was also studied using *t*-butylpyridyne (TBP) as base and TFA as acid. figure 6 shows the *J–V* characteristics of dye-sensitized solar cells with neutral, basic, and acidic electrolytes. The reference electrolyte (EL1) consists of 0.6 M 1-butyl-3-methylimidazolium iodide (BMII), 0.1 M lithium iodide (LiI), and 0.05 M iodine (I_2). The open-circuit voltage (V_{oc}) of the cell was increased upon adding 0.5 M TBP into the EL1. Contrary to the V_{oc} increase with incorporation of TBP in the electrolyte,

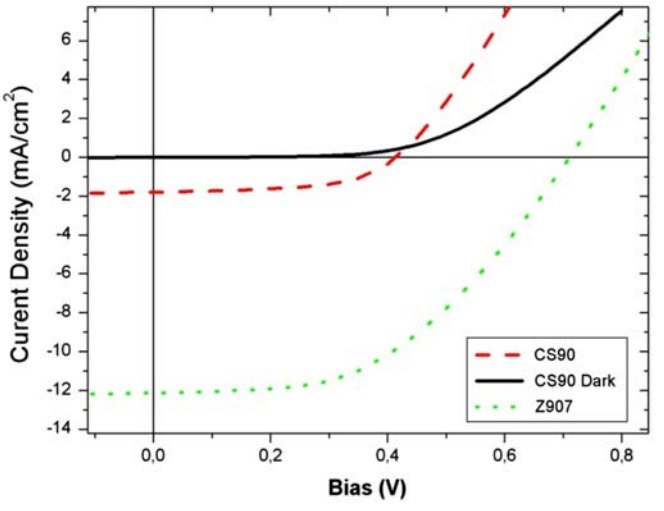

Figure 5. Current density–voltage (*J–V*) curves of *nc*-DSSCs sensitized by CS90 and Z907 measured under dark and 100 mW cm^{-2} simulated white light illumination.

Table 2. Photovoltaic performance data of CS90 and Z907 under 100 Mw cm^{-2} simulated white light illumination. I_{sc}: open-circuit voltage, V_{oc}: open-circuit voltage, FF: fill factor, I_{mp}: maximum power point current, V_{mp}: maximum power point voltage, η: efficiency.

	I_{sc} (mA cm^{-2})	V_{oc} (*V*)	FF	I_{mp} (mA cm^{-2})	V_{mp} (*V*)	η (%)
CS90	1.80	400	0.58	1.40	300	0.42
Z907	12.30	700	0.48	9.16	450	4.12

the short-circuit photocurrent density (J_{sc}) decreased. The V_{oc} increase is consistent with the dark current decrease. On the other side, V_{oc} of the cell was decreased drastically upon adding 0.5 M TFA into the EL1, whereas J_{sc} was slightly increased relative to the reference cell. Variations in V_{oc} and J_{sc} are explained in terms of a shift of the flat band potential of TiO_2. The dependence of J_{sc} on the composition of the electrolyte can also be explained on the basis of the shift of the flat band potential of TiO_2. The negative shift of flat band potential with increase in pH enables a negative shift of the conduction band (CB) edge of TiO_2, which may result in a less favorable alignment of CB of TiO_2 with LUMO of the sensitizing dye where electron injection rate slows down. V_{oc} of the cell is determined by the energy gap between the CB of TiO_2 and redox potential of the electrolyte. Negative shift of the CB edge of TiO_2 with increase in pH enables higher V_{oc}. Decreasing the pH of the electrolyte shows an opposite behavior on the TiO_2 CB [35–37].

Small variation on J_{sc} relative to V_{oc} of the cell sensitized by CS90 upon changing electrolyte pH indicates that electron injection from the dye LUMO to TiO_2 CB is less sensitive to pH changes, consistent with electrochemical data obtained from CV measurements indicating that LUMO energy level is high enough for electron injection to TiO_2 CB even at high pH. 300 mV higher reduction potential of CS90 compared to Z907

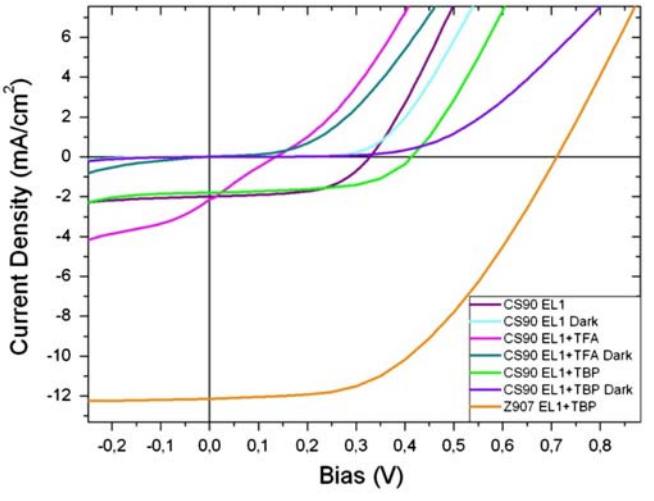

Figure 6. Current density–voltage (*J–V*) curves of *nc*-DSSCs sensitized by CS90 and Z907 and electrolyte at different pH, measured under dark and 100 mWcm^{-2} simulated white light illumination.

increases the possibility of efficient charge injection. According to previous reports by Durrant *et al.* and Lian *et al.*, addition of 0.5 M tBP in electrolyte raises the energy level of TiO_2 CB by ~200 mV which reduces injection efficiency by 10%. Efficient device performance requires only that electron injection is fast relative to excited state decay to the ground state [34]. In our case lower overall conversion efficiency of the CS90 sensitized solar cell where efficient charge separation is energetically favorable is attributed to additional limitations such as steric factors and high charge recombination ratios. Steric factors decrease TiO_2 dye interaction and raise charge recombination rates to electrolyte and dye ground states. Charge recombination to electrolyte appears not to be a significant factor in DSSC where main efficiency limiting factor is recombination to dye HOMO.

4. Conclusion

We report synthesis of heteroleptic ruthenium(II) complex containing [1-methyl-1*H*-pyridin-(2E)-ylidene]-8-quinolinamine and its application in *nc*-DSSC. Although CS90 does exhibit some potential advantages such as absorption at longer wavelengths and a lower oxidation potential, when attached to TiO_2 the electron injection is markedly worse than Z907. The spectroscopic, electrochemical, and photovoltaic evidence indicate that the steric requirements of PYE prevent optimum dye binding and restrict changes in metal complex geometry that accompany changes in oxidation state. It is therefore important to consider steric requirements of metal complex dye ligands not just to reduce the rate of chemical degradation but also their effect on binding and redox chemistry.

Acknowledgements

We acknowledge the project support funds of State Planning Organization (DPT), Ege University, University of York, and Pamukkale University.

References

[1] F. De Angelis, S. Fantacci, A. Selloni, M. Grätzel, M.K. Nazeeruddin. *Nano Lett.*, **7**, 3189 (2007).
[2] Y. Ou, G. Chen, J. Yin, G.A. Yu, S.H. Liu. *J. Coord. Chem.*, **64**, 3062 (2011).
[3] B. O'Regan, M. Gratzel. *Nature*, **353**, 737 (1991).
[4] D. Kuang, C. Klein, S. Ito, J.E. Moser, R. Humphry-Baker, N. Evans, F. Duriaux, C. Grätzel, S.M. Zakeeruddin, M. Grätzel. *Adv. Mater.*, **19**, 1133 (2007).
[5] C. Sahin, M. Ulusoy, C. Zafer, C. Ozsoy, C. Varlikli, T. Dittrich, B. Cetinkaya, S. Icli. *Dyes Pigm.*, **84**, 88 (2010).
[6] L. Zhang, G. Wen, Q. Xiu, L. Guo, J. Deng, C. Zhong. *J. Coord. Chem.*, **65**, 1632 (2012).
[7] Y.D. Lin, T.J. Chow. *J. Photochem. Photobiol. A*, **230**, 47 (2012).
[8] X. Cheng, S. Sun, M. Liang, Y. Shi, Z. Sun, S. Xue. *Dyes Pigm.*, **92**, 1292 (2012).
[9] K. Ocakoglu, F. Yakuphanoglu, J.R. Durrant, S. Icli. *Sol. Energy Mater. Sol. Cells*, **92**, 1047 (2008).
[10] C. Sahin, T. Dittrich, C. Varlikli, S. Icli, M.C. Lux-Steiner. *Sol. Energy Mater. Sol. Cells*, **94**, 686 (2010).
[11] S.H. Fan, A.G. Zhang, C.C. Ju, K.Z. Wang. *Sol. Energy*, **85**, 2497 (2011).
[12] C. Sahin, C. Tozlu, K. Ocakoglu, C. Zafer, C. Varlikli, S. Icli. *Inorg. Chim. Acta*, **361**, 671 (2008).
[13] M.K. Nazeeruddin, S.M. Zakeeruddin, J.J. Lagref, P. Liska, P. Comte, C. Barolo, G. Viscardi, K. Schenk, M. Graetzel. *Coord. Chem. Rev.*, **248**, 1317 (2004).
[14] Q. Shi, R.J. Thatcher, J. Slattery, P.S. Sauari, A.C. Whitwood, P.C. McGowan, R.E. Douthwaite. *Chem. Eur. J.*, **15**, 11346 (2009).
[15] N. Garelli, P. Vierling. *J. Org. Chem.*, **57**, 3046 (1992).
[16] C.A. Mitsopoulou, I. Veroni, A.I. Philippopoulos, P. Falaras. *J. Photochem. Photobiol., A*, **191**, 6 (2007).
[17] M.K. Nazeeruddin, A. Kay, I. Rodicio, R. Humphry-Baker, E. Mueller, P. Liska, N. Vlachopoulos, M. Graetzel. *J. Am. Chem. Soc.*, **115**, 6382 (1993).
[18] J. Slattery, R.J. Thatcher, Q. Shi, R.E. Douthwaite. *Pure Appl. Chem.*, **82**, 1663 (2010).
[19] B.J. Coe, S.J. Glenwright. *Coord. Chem. Rev.*, **203**, 5 (2000).
[20] M. Ulusoy, H. Karabıyık, R. Kılınçarslan, M. Aygün, B. Çetinkaya, S. García-Granda. *Struct. Chem.*, **19**, 749 (2008).
[21] D.S. Lamani, K.R. Venugopala Reddy, H.S. Bhojya Naik, H.R. Prakash Naik, A.M. Sridhar. *J. Macromol. Sci., Part A: Pure Appl. Chem.*, **45**, 857 (2008).
[22] K.E. Lee, M.A. Gomez, S. Elouatik, G.P. Demopoulos. *Langmuir*, **26**, 9575 (2010).
[23] W.P. Tai. *Sol. Energy Mater. Sol. Cells*, **76**, 65 (2003).
[24] K. Murakoshi, G. Kano, Y. Wada, S. Yanagida, H. Miyazoki, M. Matsumoto, S. Murasawa. *J. Electroanal. Chem.*, **396**, 27 (1995).
[25] P. Wang, S.M. Zakeeruddin, R. Humphry-Baker, J.E. Moser, M. Grätzel. *Adv. Mater.*, **15**, 2101 (2003).
[26] C. Klein, M.K. Nazeeruddin, D. Di Censo, P. Liska, M. Grätzel. *Inorg. Chem.*, **43**, 4216 (2004).
[27] T.J.J. Kinnunen, M. Haukka, T.A. Pakkanen. *J. Organomet. Chem.*, **654**, 8 (2002).
[28] G. Liu, A. Klein, A. Thissen, W. Jaegermann. *Surf. Sci.*, **539**, 37 (2003).
[29] G.C. Vougioukalakis, T. Stergiopoulos, G. Kantonis, A.G. Kontos, K. Papadopoulos, A. Stublla, P.G. Potvin, P. Falaras. *J. Photochem. Photobiol. A*, **214**, 22 (2010).
[30] C. Barolo, M.K. Nazeeruddin, S. Fantacci, D. Di Censo, P. Comte, P. Liska, G. Viscardi, P. Quagliotto, F. De Angelis, S. Ito, M. Grätzel. *Inorg. Chem.*, **45**, 4642 (2006).
[31] L.L. Okumura, N.R. Stradiotto. *Electroanalysis*, **19**, 709 (2007).
[32] E. Reisner, V.B. Arion, M.F.C. Guedes da Silva, R. Lichtenecker, A. Eichinger, B.K. Keppler, V.Y. Kukushkin, A.J.L. Pombeiro. *Inorg. Chem.*, **43**, 7083 (2004).
[33] M. Gratzel. *Inorg. Chem.*, **44**, 6841 (2005).
[34] J.E. Moser, M. Gratzel. *Chem. Phys.*, **176**, 493 (1993).
[35] T. Suresh, J. Joseph, K. Mo Son, R. Vittal, J. Lee, K.J. Kim. *Sol. Energy Mater. Sol. Cells*, **91**, 1313 (2007).
[36] S.E. Koops, B.C. O'Regan, P.R.F. Barnes, J.R. Durrant. *J. Am. Chem. Soc.*, **131**, 4808 (2009).
[37] J.B. Asbury, N.A. Anderson, E. Hao, X. Ai, T. Lian. *J. Phys. Chem. B*, **107**, 7376 (2003).